Optical Bistability in a Silicon Waveguide Distributed Bragg Reflector Fabry–Pérot Resonator

Andrew Grieco, Boris Slutsky, Dawn T. H. Tan, Steve Zamek, Maziar P. Nezhad, and Yeshaiahu Fainman

***Abstract*—We demonstrate optical bistability in a silicon waveguide Fabry–Pérot resonator formed by a pair of distributed Bragg reflectors. In the bistable regime, the output power of the resonator ceases to be uniquely determined by the input power because multiple powers within the cavity satisfy the resonance condition. Pulsating behavior is observed within the resonator output, and is attributed to noise within the experimental setup driving the resonator between the multiple allowed output powers.**

***Index Terms*—Fabry–Perot resonators, integrated optics, optical bistability.**

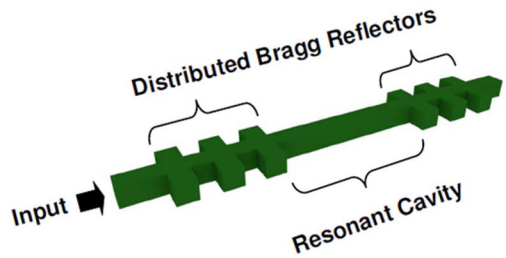

Fig. 1. Top-down diagram of a Fabry–Pérot resonator created from a pair of distributed Bragg reflectors in a strip waveguide. Note that the diagram is for conceptual purposes and is not drawn to scale.

I. Introduction

BISTABILITY occurs in devices that are composed of a material with nonlinear optical response. In the bistable regime, the output power of the device ceases to be uniquely determined by the input power because multiple powers within the cavity satisfy the resonance condition. Bistable devices are a versatile foundation for optical signal processing because they display both nonlinearity and hysteresis. This allows for the realization of photonic circuitry with functions including switching, memory, combinatorial and sequential logic, and modulation [1].

Bistable integrated photonic devices may be fabricated in a number of ways. Periodically structured dielectric waveguides [2] are an attractive solution because of their compact footprint and high packing density. However, the range of applications of this approach is limited due to high-power requirements. In contrast, resonant cavities formed from photonic crystals [3] or rings [4]–[7] are attractive because of their low-power requirements. Conversely, their application is limited due to their large footprint and low packing density.

Manuscript received March 08, 2012; revised April 18, 2012; accepted April 24, 2012. Date of publication May 24, 2012; date of current version June 06, 2012. This work was supported by the National Science Foundation (NSF), the NSF Engineering Research Center for Integrated Access Networks, Defense Advanced Research Projects Agency, and the Cymer Corporation.

A. Grieco, B. Slutsky, D. T. H. Tan, and Y. Fainman are with the Department of Electrical and Computer Engineering, University of California, San Diego, CA 92093-0407 USA (e-mail: agrieco@ucsd.edu; bslutsky@ucsd.edu; dawnth.tan@gmail.com; fainman@eng.ucsd.edu).

M. P. Nezhad is with the Department of Electrical and Computer Engineering, University of California, San Diego, CA 92093-0407 USA, and also with the Integrated Photonics Laboratory, RWTH, 52062 Aachen, Germany (e-mail: maziar@ucsd.edu).

S. Zamek was with the University of California, San Diego, CA 92093-0407 USA. He is now with KLA-Tencor Corporation, Milpitas, CA 95035 USA (e-mail: s.zamek@gmail.com).

Color versions of one or more of the figures in this paper are available online at http://ieeexplore.ieee.org.

Digital Object Identifier 10.1109/JLT.2012.2197731

In this paper, we propose and demonstrate optical bistability in a waveguide Fabry–Pérot resonator created from a pair of distributed Bragg reflectors [8] within a strip waveguide (see Fig. 1). This design has the advantage of maintaining the small footprint and high packing density of a periodically structured dielectric waveguide [9], while taking advantage of the reduced power consumption featured in devices based on resonant cavities. The packing density advantage is especially significant in applications that might require long cavity, small free spectral range resonators for narrowband filtering [10]. At the opposite extreme, Fabry–Perot topology is also appropriate for very short cavities, since it does not suffer from bending loss that limits the radius of resonant rings. Furthermore, due to the utilization of distributed Bragg reflectors, the configuration presented here is particularly attractive for wavelength selective applications such as wavelength division multiplexing. Bragg reflectors can also implement certain signal processing functions, including broadband filtering and engineered dispersion [11], with little effect on the device footprint. The implementation of signal processing functions using ring resonators often requires a cascade of multiple rings [12], [13], significantly increasing the footprint. Therefore, the development of an experimental understanding of bistable behavior in this type of device is valuable.

II. Experimental Design and Fabrication

The device is fabricated on a silicon-on-insulator (SOI) substrate with a 3 μm buried oxide layer and a 250 nm top silicon layer. The substrate is spin coated with hydrogen silsesquioxane (HSQ) resist that is patterned via electron beam lithography, and developed so that it forms a mask with the lateral dimensions of the desired waveguide. The substrate then undergoes an inductively coupled plasma reactive ion etch process that removes the silicon not protected by the HSQ mask. The patterned silicon is then cladded with a layer of silicon dioxide deposited via plasma-enhanced chemical vapor deposition.

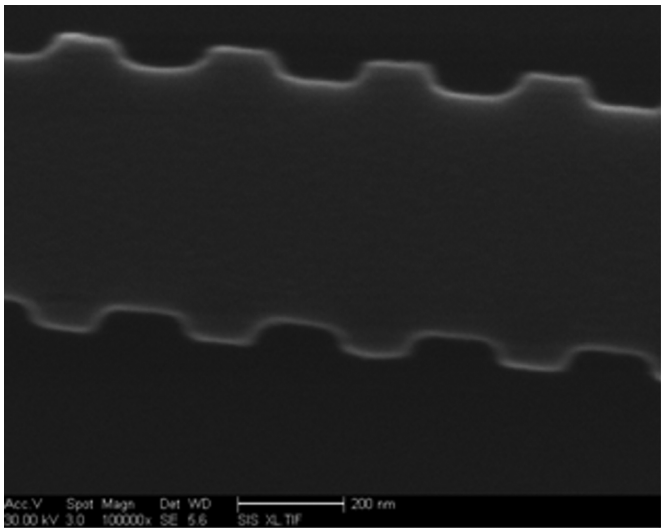

Fig. 2. Scanning electron micrograph of an uncladded section of the SOI strip waveguide distributed Bragg reflector employed in this experiment. Note that the scale bar label is 200 nm.

The nominal dimensions of the silicon strip waveguide employed in this experiment are 500 nm width and 250 nm height. The Bragg grating mirrors are formed by periodically modulating the waveguide width by ± 50 nm (see Fig. 2). The grating period is 0.304 μm, and the mirrors are 94 periods long. The mirrors are separated by a distance of 200.225 μm. Nanotaper couplers are employed at both the input and output terminals of the device [14].

Characterization of the device was performed using the experimental setup illustrated in Fig. 3. The laser source (Agilent model 81980A) is fiber coupled to a polarization scrambler, a fiber polarizer, and a polarization-maintaining lensed fiber oriented to excite the TE mode in the silicon waveguide. The light transmitted through the sample is collected by a 0.4 NA microscope objective (Lens 1 in Fig. 3) and imaged onto the detector by two sequentially arranged 4F systems (lenses 1–2 and 3–4). An iris in the first focal plane eliminates stray light from around the waveguide endpoint. A polarizer in the second Fourier plane rejects any quasi-TM mode component that may arise from imperfect alignment of the lensed fiber or from waveguide defects. The detector and power meter are Newport model 918D-IG-OD3 and 2931-C, respectively. The measurements are automated by a computer which controls the laser source and power meter. For the measurements in this paper, input laser power refers to the power exiting the laser source, while transmission power refers to the power registered by the detector.

III. Measurement and Discussion

The device power transmission spectrum of the quasi-TE mode (defined such that the electric field vector is parallel to the substrate) within the stop band of the distributed Bragg reflectors is shown in Fig. 4. The free spectral range of the transmission peaks is 1.33 nm. In the linear regime, the resonator has a maximum peak-to-trough signal rejection of 23.3 dB around the $\lambda \sim 1547$ nm resonance. The full-width at half-maximum bandwidth of this resonance is $\lambda_{\mathrm{FWHM}} = 0.080$ nm. The

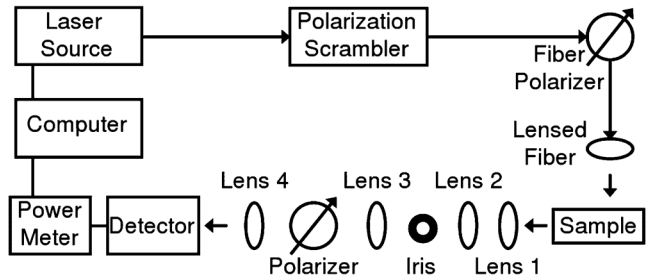

Fig. 3. Experimental setup used to characterize the device. The details of the components used may be found in the text.

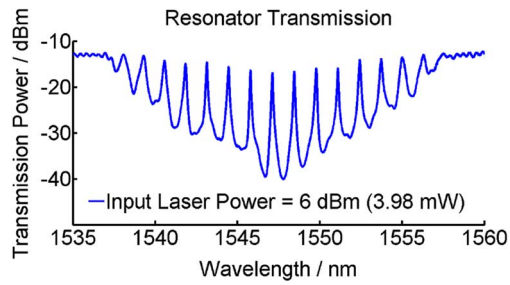

Fig. 4. Transmission of the quasi-TE mode of the distributed Bragg reflector Fabry–Pérot resonator.

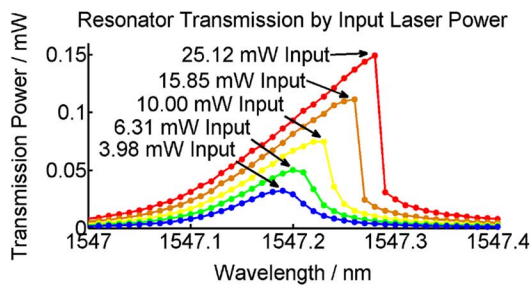

Fig. 5. Power dependence of the transmission around the 1547 nm resonance peak of the quasi-TE mode of the distributed Bragg reflector Fabry–Pérot resonator.

quality factor corresponding to these measurements, defined as $Q = \lambda/\lambda_{\mathrm{FWHM}}$, exceeds 19 000.

The power dependence of the transmission spectrum of the quasi-TE mode around the 1547 nm resonance peak as a function of continuous wave input power is shown in Fig. 5. As the input power is increased, the resonant peak becomes asymmetrical and displays an abrupt transition from the peak power. This behavior is indicative of resonator bistability [4]–[6].

The effects that contribute to the power dependence of the device resonance are the third-order material nonlinearity [15], the free-carrier dispersion effect [16], the thermo-optic effect [17], [18], and thermal expansion [18], [19] (both through altering the length of the resonant cavity and by altering the effective index through geometrical distortion of the waveguide). It has been previously demonstrated that thermal effects dominate free-carrier dispersion by a wide margin for continuous wave pumping in SOI waveguides [7]. This may be cursorily verified by observing the direction of nonlinear index change. Likewise, among the remaining effects, it can be shown that the thermo-optic effect dominates both the material nonlinearity [20] and thermal expansion [6].

A theoretical model of the response of a silicon waveguide Fabry–Pérot resonator is developed following those of prior authors [21], [22]. Of particular interest, the steady-state relationship between the input and output intensities of the resonator may be expressed as

$$I_{\rm in} = I_{\rm tr}\frac{|1 - R\exp(-L\alpha)\exp(-{\rm i}\phi)|^2}{T^2\exp(-L\alpha)} \quad (1)$$

$$\phi = 2L\beta + \frac{3I_{\rm tr}n_{2,\rm eff}\beta_0[1-\exp(-L\alpha)][\exp(L\alpha)+R]}{T\alpha} \quad (2)$$

where $I_{\rm in}$ is the intensity input into the resonator, $I_{\rm tr}$ is the intensity transmitted by the resonator, R is the mirror reflectance, T is the mirror transmittance, L is the resonant cavity length, α is the net waveguide attenuation constant, β is the propagation constant of the guided radiation, β_0 is the free space propagation constant, and $n_{2,\rm eff}$ is the effective nonlinear index coefficient of the guided mode. To arrive at this equation, effects resulting from two photon absorption, free-carrier dispersion, and thermal expansion are neglected. For the device at hand, these approximations are justified.

Bistable behavior arises in the resonator response because, under certain conditions, (1) yields multiple distinct solutions $I_{\rm tr}$ for a given $I_{\rm in}$. The resonator can then switch randomly between these solutions under the influence of noise (both amplitude [4]–[7] and phase [23]). Experimental evidence of this random switching behavior in the Fabry–Pérot resonator is presented in Fig. 6. The solid curve in the figure shows a model of the device response following (1) and (2) with parameters $R = 0.866, T = 0.104, L = 200.225\ \mu$m, $\alpha = 5$ dB/cm, $\beta_0 = 4.06066\ \mu{\rm m}^{-1}$, $\beta = 10.4017\ \mu{\rm m}^{-1}$, and $n_{2,\rm eff} = 7.82\times10^{-11}$ cm^2/W. Of these, R, T, and α are extracted from the low-power spectrum in Fig. 4, and β_0 is the known wavenumber of the laser source. The thermo-optic effect is represented by $n_{2,\rm eff}$. To determine $n_{2,\rm eff}$, it is necessary to estimate the optical power inside the waveguide (which depends on the coupling efficiency), the fraction of power that is absorbed and converted to heat, and the rate of heat dissipation [20]. Here, the coupling loss is taken to be -18 dB and the collection efficiency to be 92.4%. These values are consistent what we typically observe in similar devices, and yield a good fit to the data in Fig. 6. The fitting of data in Fig. 6 also yields the absorption coefficient $\alpha_{\rm abs} = 1$ dB/cm and thermal dissipation time constant $\tau_{\rm th} = 2.26\ \mu$s. It is pertinent to note that the mechanisms of both absorption [24] and heat dissipation [25] in on-chip waveguides are still the subjects of active research. The exact value of β is also chosen for best fit in Fig. 6. This value varies somewhat with the ambient temperature between measurements and therefore cannot be obtained directly from the low-power spectrum in Fig. 4. Silicon material properties used to compute $n_{2,\rm eff}$ are 1.86×10^{-4} K^{-1} for the thermo-optic coefficient [6], 2.3×10^{-3} kg/cm^3 for the density of Si [7], 705 J/(kg $\times$ K) for the thermal capacity of Si [7], and 6×10^{-14} cm^2/W for the nonlinear index coefficient of Si [15]. The nonlinearity of the SiO_2 cladding is so small that it is neglected in the analysis [6].

The sensitivity of the model to the waveguide parameters provides insight into the origin of the pulsating behavior of the device. The dominant nonlinearity within the experiment arises from the thermo-optic effect, which is driven by absorption of the laser source and subsequent heating of the device. We attribute the switching between the two stable states on the hysteresis curve to the random variation of laser output that can occur as the laser is being tuned from one power level to another and its internal feedback controller is searching for an equilibrium. The laser operating manual does not provide specifications on transient power variation in the laser output, and due to the bandwidth limitations of the measurement system we are unable to perform this characterization. However, a compelling argument can be made in favor of this attribution through the elimination of other possible noise sources. We note that the specified maximum drift in laser power when operated at constant output is $\pm0.23\%$ per hour (typically much less), which is insignificant and may be excluded as a source of switching.

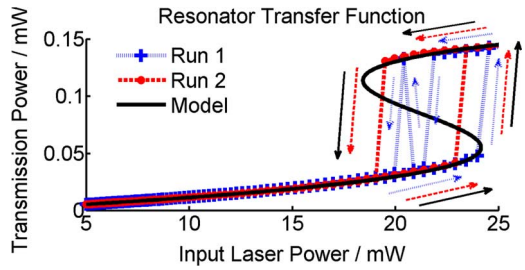

Fig. 6. Measurements and theoretical response of the transfer function of the quasi-TE mode of the distributed Bragg reflector Fabry–Pérot resonator. Run 1 and Run 2 were made 8 min apart. Point-by-point measurements are taken at an average rate of 0.77 Hz. The wavelength detuning from resonance of the model is 0.15 nm.

In principle, drift in ambient temperature could also trigger a switch. This may be excluded as a factor by observing the repeatability, both between subsequent runs and within the back and forth sweeps of a single run, in Fig. 6. On the time scale of the experiment, ambient temperature drift will be monotonic in nature. Had any such drift occurred, it would have spoiled the repeatability of the nonbistable portion of the data. Furthermore, as all of the measurements lie on the outside of the hysteresis loop, the source of switching must only occur in between the point-by-point measurements. Had the switching occurred during the detector integration time ($\sim$0.25 ms), it would have resulted in data points that appear to lie within the hysteresis loop. This is because the high-power and low-power portions of the measurement would average to some intermediate power value.

The anticipated magnitude of temperature changes is also too small to trigger a switch. The maximum magnitude of thermal drift observed in the laboratory environment is 0.1 °C/min (typically much less). Since the thermo-optic coefficient of the waveguide effective index is approximately equal to that of silicon, the maximum change in ambient temperature modifies the guide effective index by $\sim1.86\times10^{-5}$ per minute. This is much less than the $\sim3\times10^{-4}$ index difference in the resonator between the high-power and low-power bistable states, and is trivial over the point-by-point measurement time.

IV. Conclusion

In conclusion, we have demonstrated optical bistability in a silicon waveguide distributed Bragg reflector Fabry–Pérot res-

onator. The behavior arises primarily from the thermo-optic effect. At high input powers, evidence for pulsating behavior in the resonator was observed. This behavior is attributed to noise within the experimental setup driving the resonator between bistable states. The device combines the small footprint and high packing density associated with linear dielectric waveguides with the reduced power consumption associated with resonant structures. Productive areas of future research include performing a time-dependent stability analysis of the device. This could be expected to produce strategies to mitigate instability, and would be particularly attractive from a signal processing perspective [10].

ACKNOWLEDGMENT

The authors would like to thank the Nano3 Staff at UCSD and B. Mitchell at UCSB for their support during sample fabrication, and C. Hennessey for logistical support.

REFERENCES

[1] H. M. Gibbs, *Optical Bistability: Controlling Light With Light*. New York: Academic, 1985.
[2] N. D. Sankey, D. F. Prelewitz, and T. G. Brown, "All-optical switching in a nonlinear periodic-waveguide structure," *Appl. Phys. Lett.*, vol. 60, pp. 1427–1429, Mar. 1992.
[3] K. Ikeda and Y. Fainman, "Nonlinear Fabry–Perot resonator with a silicon photonic crystal waveguide," *Opt. Lett.*, vol. 31, pp. 3486–3488, Dec. 2006.
[4] V. R. Almeida and M. Lipson, "Optical bistability on a silicon chip," *Opt. Lett.*, vol. 29, pp. 2387–2389, Oct. 2004.
[5] G. Priem, P. Dumon, W. Bogaerts, D. Van Thourhout, G. Morthier, and R. Baets, "Optical bistability and pulsating behaviour in silicon-on-insulator ring resonator structures," *Opt. Exp.*, vol. 13, pp. 9623–9628, Nov. 2005.
[6] P. Sun and R. M. Reano, "Low-power optical bistability in a free-standing silicon ring resonator," *Opt. Lett.*, vol. 35, pp. 1124–1126, Apr. 2010.
[7] Q. Xu and M. Lipson, "Carrier-induced optical bistability in silicon ring resonators," *Opt. Lett.*, vol. 31, pp. 341–343, Feb. 2006.
[8] H.-C. Kim, K. Ikeda, and Y. Fainman, "Tunable transmission resonant filter and modulator with vertical gratings," *J. Lightw. Technol.*, vol. 25, no. 5, pp. 1147–1151, May 2007.
[9] S. Zamek, D. T. H. Tan, M. Khajavikhan, M. Ayache, M. P. Nezhad, and Y. Fainman, "Compact chip-scale filter based on curved waveguide Bragg gratings," *Opt. Lett.*, vol. 35, pp. 3477–3479, Oct. 2010.
[10] Y. Wang, A. Grieco, B. Slutsky, B. Rao, Y. Fainman, and T. Nguyen, "Design and analysis of a narrowband filter for optical platform," in *Proc. 36th Int. Conf. Acoust., Speech Signal Process. (IEEE)*, Prague, Czech Republic, May 2011, pp. 1633–1636.
[11] D. T. H. Tan, K. Ikeda, R. E. Saperstein, B. Slutsky, and Y. Fainman, "Chip-scale dispersion engineering using chirped vertical gratings," *Opt. Lett.*, vol. 33, pp. 3013–3015, Dec. 2008.
[12] F. Xia, M. Rooks, L. Sekaric, and Y. Vlasov, "Ultra-compact silicon WDM optical filters with flat-top response for on-chip optical interconnects," in *Proc. Conf. Lasers Electro-Opt./Quantum Electron. Laser Sci. Conf. Photon. Appl. Syst. Technol.*, Baltimore, MD, May 6, 2007, pp. 1–2.
[13] M. L. Cooper, G. Gupta, M. A. Schneider, W. M. J. Green, S. Assefa, F. Xia, Y. A. Vlasov, and S. Mookherjea, "Statistics of light transport in 235-ring silicon coupled-resonator optical waveguides," *Opt. Exp.*, vol. 18, pp. 26505–26516, Dec. 2010.
[14] V. R. Almeida, R. R. Panepucci, and M. Lipson, "Nanotaper for compact mode conversion," *Opt. Lett.*, vol. 28, pp. 1302–1304, Aug. 2003.
[15] M. A. Foster, A. C. Turner, J. E. Sharping, B. S. Schmidt, M. Lipson, and A. L. Gaeta, "Broad-band optical parametric gain on a silicon photonic chip," *Nature*, vol. 441, pp. 960–963, Jun. 2006.
[16] R. A. Soref and B. R. Bennett, "Electrooptical effects in silicon," *J. Quantum Electron.*, vol. QE-23, pp. 123–129, Jan. 1987.
[17] G. Cocorullo and I. Rendina, "Thermo-optical modulation at 1.5 μm in silicon etalon," *Electron. Lett.*, vol. 28, pp. 83–85, Jan. 1992.
[18] Z. Tan and J. Arndt, "Temperature dependence of refractive index of glassy SiO_2 in the infrared wavelength range," *J. Phys. Chem. Solids*, vol. 61, pp. 1315–1320, Aug. 2000.
[19] Y. Okada and Y. Tokumaru, "Precise determination of lattice parameter and thermal expansion coefficient of silicon between 300 and 1500 K," *J. Appl. Phys.*, vol. 56, pp. 314–320, Jul. 1984.
[20] , R. W. Eason and A. Miller, Eds., *Nonlinear Optics in Signal Processing*. London, U.K.: Chapman & Hall, 1993, p. 156.
[21] S. Li and K. T. Chan, "Optical bistability in an all-optical fiber nonlinear Fabry–Perot resonator with linear absorption," *Fiber Integr. Opt.*, vol. 16, pp. 407–413, 1997.
[22] M. Tien, J. F. Bauters, M. J. Heck, D. J. Blumenthal, and J. E. Bowers, "Ultra-low loss Si_3N_4 waveguides with low nonlinearity and high power handling capability," *Opt. Exp.*, vol. 18, pp. 23562–23568, Nov. 2010.
[23] F. A. Hopf, P. Meystre, P. D. Drummond, and D. F. Walls, "Anomalous switching in dispersive optical bistability," *Opt. Commun.*, vol. 31, pp. 245–250, Nov. 1979.
[24] M. Borselli, T. J. Johnson, and O. Painter, "Accurate measurement of scattering and absorption loss in microphotonic devices," *Opt. Lett.*, vol. 32, pp. 2954–2956, Oct. 2007.
[25] M. Brunstein, R. Braive, R. Hostein, A. Beveratos, I. Robert, I. Sagnes, P. Monnier, F. Raineri, V. Moreau, A. Yacomotti, R. Raj, and A. Levenson, "Thermal dissipation dynamics in an optically pumped photonic crystal nano-cavity," presented at the presented at the Conf. Lasers Electro-Opt./Int. Quantum Electron. Conf., Baltimore, MD, May 31, 2009, Paper CFP2.

Authors, biographies not available at the time of publication.